Mesoporous Nickel/Nickel Oxide—a Nanoarchitectured Electrode

Phillip A. Nelson, Joanne M. Elliott,† George S. Attard, and John R. Owen*

Department of Chemistry, University of Southampton, Highfield, Southampton SO17 1BJ, United Kingdom

Received January 31, 2001. Revised Manuscript Received November 2, 2001

Metallic nickel was electrodeposited from aqueous nickel(II) acetate dissolved in the lyotropic liquid crystalline phases of Brij 56 and Brij 78 surfactant templates to form metal films with hexagonal arrays of nanometer-sized channels. The applicability of these materials as inexpensive, large area and low-resistance current collectors was demonstrated by cyclic voltammetry. The redox charge capacity of the surface oxide in aqueous KOH was enhanced by 2 orders of magnitude over that of a nontemplated sample with no detectable impedance of the reaction rate.

Introduction

Nickel is an important material in electrochemical technology which is used widely as an electrode material in batteries[1] (e.g., cadmium−nickel oxide, zinc−nickel oxide, metal hydride−nickel oxide, and hydrogen−nickel oxide), fuel cells,[2,3] alkaline water electrolysis,[4] and electrochemical hydrogenation of organic species.[5] In such cases, the performance of the electrode is proportional to its electrochemically active surface area since the reactions involved are inherently surface processes. Consequently, improvements in nickel electrode technology have generally resulted from improvements in the active surface area of electrode materials. At present, high surface area nickel electrodes are prepared via several routes. Synthesis of sintered microporous nickel films involves mixing nickel powder, consisting of micrometer-sized particles, with an organic binder which subsequently undergoes thermal decomposition and sintering. Nanoporous Raney nickel is produced by using a number of methods, the most common of which is cathodic co-deposition of the Raney nickel precursor alloys (Ni/Al or Ni/Zn) on a conducting support. Nickel has also been electrodeposited into the voids of a microporous polymer matrix template. Subsequent heat treatment, to burn out the polymer, produced microporous nickel coatings.[6] In these cases, fabrication of the porous nickel film involves either a thermal treatment step or leaching with concentrated alkali solutions. In all cases, the structures formed possess disordered porosity with voids of varying cross section interconnected by narrower intervoid spaces. While possessing high surface areas, the disordered porosity of these materials acts to impede the movement of gaseous and liquid species through the pore network. By contrast, materials with high surface areas and a uniform, ordered pore network would be expected to exhibit superior performance in electrochemical systems which rely on gas or liquid diffusion within the electrode material. Ordered macroporous nickels have been produced previously,[7] but in these cases, the repeat distances, in the submicron range, were too large to produce greatly enhanced surface areas.

In 1992, researchers at the Mobil Corporation reported the first synthesis of mesoporous silica and aluminosilicates.[8] Their synthetic approach was based on the self-assembly of a cationic surfactant into micelles that acted as a template for the formation of the porous oxide network. Since then, interest in materials possessing ordered porous networks with uniform pore diameters in the nanometer range has intensified significantly, motivated by the desire to replace conventional porous materials fabricated by methods such as powder metallurgy and plasma sputtering. This new class of materials is expected to afford superior mass transport properties and enhanced surface areas in comparison with conventional porous materials, making them attractive for application in catalysis, selective separation, and electrochemical devices such as batteries and fuel cells.

Since 1992, mesostructural templating techniques have been extended with the use of other amphiphilic species such as block copolymers,[9] primary amines,[10]

* To whom correspondence should be addressed. E-mail: jro@soton.ac.uk.

† Present address: Department of Chemistry, University of Reading, Whiteknights, Reading RG6 6AH, U.K.

(1) Vincent, C. A.; Scrosati, B. *Modern Batteries- An Introduction to Electrochemical Power Sources*, 2nd ed.; Arnold: London, 1997.

(2) Al-Saleh, M. A.; Sleem-Ur-Rahman; Kareemuddin, S. M. M. J.; Al-Zakri, A. S. *J. Power Sources* **1998**, *72*, 159.

(3) Kiros, Y.; Schwartz, S. *J. Power Sources* **2000**, *87*, 101.

(4) Sealey, S. *Modern Chlor-alkali Technology*; Royal Society of Chemistry: Cambridge, 1998; Vol. 7.

(5) Anantharaman, V.; Pintauro, P. N. *J. Electrochem. Soc.* **1994**, *141* (10), 2729.

(6) Brown, I. J.; Sotiropoulos, S. *J. Appl. Electrochem.* **2000**, *30*, 107.

(7) (a) Jiang, P.; Cizeron, J.; Bertone, J. F.; Colvin, V. L. *J. Am. Chem. Soc.* **1999**, *121*, 7957−7958. (b) Yan, H. W.; Blanford, C. F.; Holland, B. T.; Parent, M.; Smyrl, W. H.; Stein, A. *Adv. Mater.* **1999**, *11*, 1003−1006. (c) Xu, L. B.; Zhou, W. L. L.; Frommen, C.; Baughman, R. H.; Zakhidov, A. A.; Malkinski, L.; Wang, J. Q. *Chem. Commun.* **2000**, 997.

(8) Kresge, C. T.; Leonowicz, M. E.; Roth, W. J.; Vartuli, J. C.; Beck, J. S. *Nature* **1992**, *359*, 710.

(9) Yang, P.; Zhao, D.; Margolese, D. I.; Chmelka, B. F.; Stucky, G. D. *Nature* **1998**, *396*, 152.

10.1021/cm011021a CCC: $22.00
Published on Web 01/12/2002

and poly(ethylene oxide) surfactants[11] to the fabrication of a range of silicate and non-silicate oxides. These syntheses were carried out at surfactant concentrations much lower (usually <7 wt % surfactant) than those required to produce bulk, lyotropic liquid crystalline phases.

Attard et al.[12−13] have developed a different approach to organic structural templating. This uses high surfactant concentrations (>30 wt % surfactant) to form an homogeneous self-assembled liquid crystal template. The inorganic material is formed in the aqueous domains of the template; however, because the liquid crystalline phases are present prior to and throughout the synthesis, this technique affords the ability to predict the final structure of the inorganic product. Another major advantage of the liquid crystalline templating approach is the ability to fabricate thin films via electrodeposition. Attard et al.[14] have used the method to produce platinum thin films which are nanoarchitectured by electroreduction of hexachloroplatinic acid within the aqueous domains of a liquid crystal. Similarly, Whitehead and co-workers[15] used a liquid crystal templating route to synthesize mesoporous films of metallic tin by electroreduction of a Sn(II) salt within the aqueous domains of an hexagonal (H_1) liquid crystalline mesophase.

We have exploited the structure-directing properties of lyotropic liquid crystalline phases to produce mesoporous nickel films via electrodeposition. The hexagonal mesophases of two poly(ethylene oxide) based surfactants were used to direct the deposition of nickel by electroreduction of a Ni(II) salt in the aqueous domains of the liquid crystalline phases. This represents the first synthesis of mesoporous nickel via the liquid crystal templating electrodeposition route. The significance of this work lies in the fact that for the first time, we have used this route to synthesize a commercially important, relatively inexpensive metal/metal oxide with high surface areas using the inexpensive and commercially available Brij surfactants.

Experimental Section

Liquid Crystalline Templating Mixtures. The nonionic surfactants Brij 56 ($C_{16}[EO]_n$ where $n \sim 10$) and Brij 78 ($C_{18}[EO]_n$ where $n \sim 20$) were obtained from Aldrich and used as received. The precursor solution used in electroreduction consisted of nickel(II) acetate tetrahydrate (Fluka, >99%), sodium acetate trihydrate (Fluka, >99.5%), and boric acid (BDH Chemicals, >99.5%). All solutions were prepared using deionized water, and glassware was cleaned by soaking in a 3% solution of Decon 90 (Hogg) for 24 h and subsequent rinsing with deionized water.

The templating media used in the electrodeposition of mesoporous nickel were binary systems comprised of either Brij 56 or Brij 78 surfactants and an aqueous solution consisting of 0.2 M nickel acetate, 0.5 M sodium acetate, and 0.2 M boric acid. In the preparing of the mixtures, the surfactant was heated to ~60 °C (above its melting point) in a glass vial and mixed manually using a glass rod on addition of the aqueous solution. Mixing times of ~10 min were required to obtain an homogeneous mixture. Complete mixing was confirmed by homogeneity of the color of the liquid crystals and by the absence of macroscopic surfactant particles under the nonpolarizing light of an optical microscope. Phase diagrams of the templating media, in the composition range of 30−85 wt % Brij, were investigated using an Olympus BH-2 polarizing microscope equipped with a Linkam TMS 90 heating/cooling stage accurate to ±0.1 °C. Here, thin films of the liquid crystals were prepared by sandwiching the mixture between a glass microscope slide and cover slip. Liquid crystalline phases were identified based on their optical texture,[16] viscosity, and the shape of the air bubbles present in the mixture.

Electrodeposition. Electrochemical experiments were conducted using a purpose-built potentiostat and potential ramp generator with a three-electrode cell consisting of a gold working electrode, a saturated calomel reference electrode (SCE), and a platinum gauze counter electrode. Electrochemical synthesis and characterization was carried out in Pyrex water-jacketed cells. Cell temperature was maintained at 25 °C with an accuracy of ±0.1 °C using a Grant ZD thermostated water bath.

Nickel films were electrodeposited at a constant potential of −0.9 V vs SCE from a 65 wt % surfactant/electrolyte solution mixture. Films grown for transmission electron microscopy (TEM) and X-ray diffraction (XRD) analysis were deposited onto approximately 3 cm^2 thin film gold electrodes made by evaporation of gold onto chromium-coated glass microscope slides. The electrodes were cleaned in an ultrasonic bath of 2-propanol for 60 min prior to deposition, rinsed with deionized water, and dried under ambient conditions. Films used in electrochemical characterization were deposited onto 1 mm gold disks encased in an epoxy insulator. These were cleaned by first polishing consecutively on 25 μm, 1 μm, and 0.3 μm alumina-embedded (obtained from Buehler) microcloths and cycling the electrodes between −0.2 and 1.8 V vs SCE at 200 mV s^{-1} for 5 min in a 2 M H_2SO_4 solution. With each cycle, a monolayer of gold oxide was formed and subsequently removed from the electrode surface.[17]

Characterization. Structural characterization of the films was carried out to confirm the templating effect of the liquid crystal on the deposit morphology. TEM was performed on a JEOL 2000FX TEM working at 200 kV. XRD was carried out using a Siemens D-5000 diffractometer (Cu K_α radiation) with a 2θ range of 1−5° and a scan rate of 5° min^{-1}.

Electrochemical characterization was performed immediately after washing for 24 h in 2-propanol and then water, with minimum exposure to air before immersing in the 3 M or 6 M KOH used for the voltammetry. After the open circuit potential was measured, the potential was first held at −1.15 V vs SCE for 10 min to reduce any oxide that may have formed during washing. The nickel was then cycled between −1.3 and +0.5 V vs SCE, starting in the anodic direction from −1.3 V.

Results and Discussion

Phase Characterization. Both the Brij 56 and Brij 78 liquid crystal templating mixtures were found to exhibit a variety of structural phase morphologies. The phase diagram of Brij 56 with the nickel(II) acetate deposition solution is shown in Figure 1 and indicates relatively complex lyotropic phase behavior. In general, only the hexagonal (H_I) and bicontinuous cubic (V_I) phases were of interest in our liquid crystal templating

(10) Tanev, P. T.; Pinnavaia, T. J. *Science* **1995**, *267*, 865.
(11) Bagshaw, S. A.; Prouzet, E.; Pinnavaia, T. J. *Science* **1995**, *269*, 1242.
(12) Attard, G. S.; Glyde, J. C.; Goltner, C. G. *Nature* **1995**, *378*, 366.
(13) Attard, G. S.; Edgar, M.; Goltner, C. G. *Acta Mater.* **1998**, *46* (3), 751.
(14) Attard, G. S.; Bartlett, P. N.; Coleman, N. R. B.; Elliott, J. M.; Owen, J. R.; Wang, J. H. *Science* **1997**, *278*, 838.
(15) Whitehead, A. H.; Elliott, J. M.; Owen, J. R.; Attard, G. S. *Chem. Commun.* **1999**, 331.
(16) Mitchell, D. J.; Tiddy, G. J. T.; Waring, L.; Bostock, T.; McDonald, M. P. *J. Chem. Soc., Faraday Trans. 1* **1983**, *79*, 975.
(17) Angerstein-Kozlowska, H.; Conway, B. E.; Hamelin, A.; Stoicoviciu, L. *Electrochim. Acta* **1986**, *31*, 1.

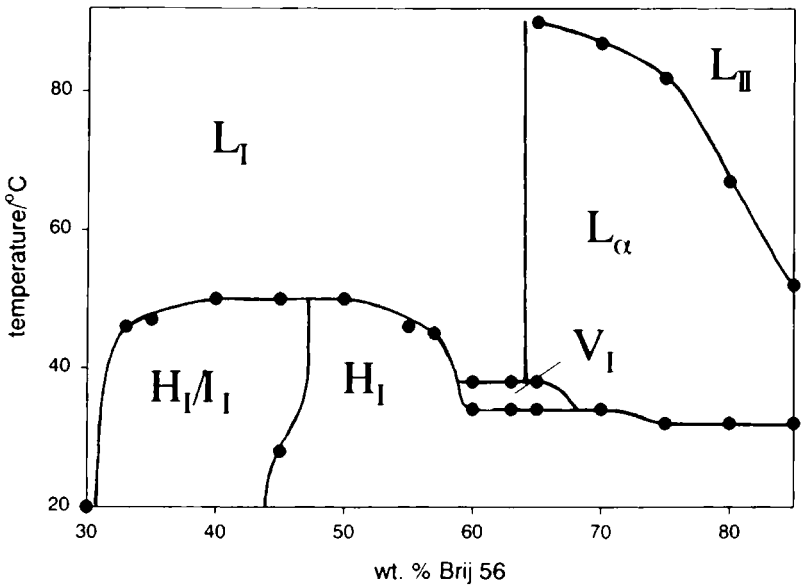

Figure 1. Liquid crystalline phase diagram of the Brij 56/0.2 M nickel(II) acetate, 0.5 M sodium acetate, 0.2 M boric acid templating system as determined by polarizing light microscopy shows lyotropic phase behavior.

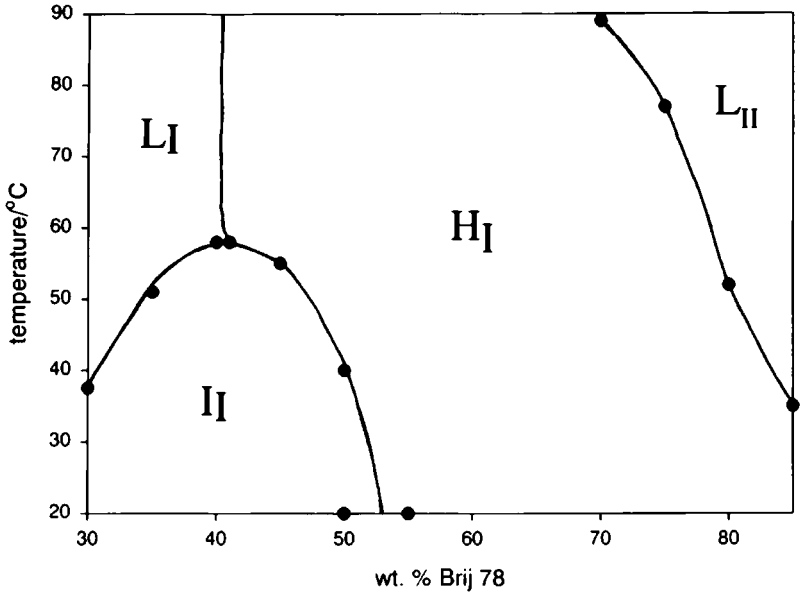

Figure 2. Liquid crystalline phase diagram of the Brij 78/0.2 M nickel(II) acetate, 0.5 M sodium acetate, 0.2 M boric acid templating system as determined by polarizing light microscopy also shows lyotropic phase behavior.

syntheses since only these phases are capable of producing materials with continuous pore networks and adequate mechanical stability. Figure 1 shows a large stable H_I domain, enabling fabrication of H_I structures over a range of temperatures and compositions using this templating system. The synthesis of V_I nickel is somewhat more restricted in that its fabrication is limited to surfactant concentrations between 60 and 65 wt % in the temperature range of 34−38 °C. In comparison with the Brij 56/water system,[18] the lamellar (L_α) phase region of the Brij 56 templating mixture is slightly enlarged at the expense of the H_I and hexagonal/cubic micellar (H_1/I_I) phase regions. The introduction of the deposition solution ions to the Brij 56/water system also results in the stabilization of the small V_I domain at lower temperatures than that observed for the Brij 56/water system.

The Brij 78 templating system is somewhat simpler in its phase behavior than the Brij 56 system. Figure 2 shows an enlarged H_I domain that is stable over a large temperature and composition range. The Brij 78 phase behavior was found to be less sensitive to the addition of the deposition solution ions than was the Brij 56 system in that the phase diagram of the Brij 78 templating solution varied only slightly from that of the Brij 78/water system.

TEM and XRD. The porosity of liquid crystal templated nickel was investigated using TEM. Figure 3 shows the mesostructure of nickel templated from the H_1 phase of a Brij 56 liquid crystal template. We note that the TEM micrographs do not show direct evidence of an hexagonal nanostructure. Indeed, the images could be construed as showing a lamellar structure. This is considered to be very unlikely, because the formation of the lamellar phase of the template requires higher concentrations of surfactant and much higher temper-

(18) Coleman N. Ph.D. Thesis, University of Southampton, 1999.

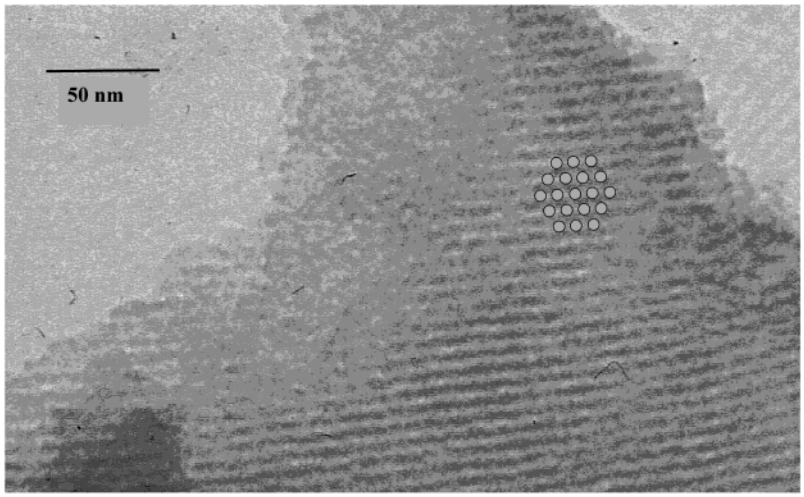

Figure 3. TEM of Brij 56 templated nickel showing the ordered mesoporosity of the H_I structure. Nickel was electrodeposited at 25 °C and −900 mV vs SCE. (The overlaid hexagonal pattern shows the structure of the template.)

atures, as indicated in the phase diagram (Figure 1). In this case, direct observation of an hexagonal pattern of channels "end-on" was not possible because of difficulties due to the ferromagnetism of nickel. However, the TEM image is consistent with previous observations of hexagonally oriented channels of other H_1 materials prepared by electrodeposition, in which the images of neighboring pores were superimposed if the pores were not exactly parallel to the beam axis.[19] In the extreme case of particles viewed laterally, at 90° to the pore axis, the same pattern can be expected. The center-to-center pore spacing was calculated to be 5.2 ± 1.0 nm assuming an hexagonal nanostructure with the use of the appropriate trigonometric conversion (i.e., the line spacing measured directly from the TEM and multiplied by $2/(3)^{1/2}$). The mesoporosity of the nickel structures produced from the Brij 56 surfactant is well-ordered, and channels have long range continuity. There are no visible necks or blockages in the channels which might retard mass transport within the pores and limit the electrochemically accessible surface area.

Low-angle XRD results from Brij 56 templated nickel support TEM data. Figure 4a shows a typical XRD pattern for mesostructured nickel using the H_1 mesophase of Brij 56 as the structure-directing agent. The strong, sharp peak indicates a mesoscopic order with a *d* spacing of 7.0 ± 0.7 nm, corresponding to a pore-to-pore separation of 8.1 ± 0.8 nm. The value larger than that determined by TEM is, as yet, unexplained but is in accordance with previous work on mesoporous cobalt.[19] Nickel mesostructures templated from the hexagonal phase of a Brij 78 liquid crystal showed similar XRD patterns as shown in Figure 4b. It has a *d* spacing of 7.7 ± 0.7 nm. As expected, the use of a larger surfactant molecule ($C_{18}[EO]_{20}$ as compared with $C_{16}[EO]_{10}$) caused an increase in the periodicity of the resulting mesostructure. The lower intensity may be due to an increased polydispersity of the Brij 78 sample. The higher background is a typical result of sample surface inhomogeneity and imperfect alignment, both of which become problematic at very low angles.

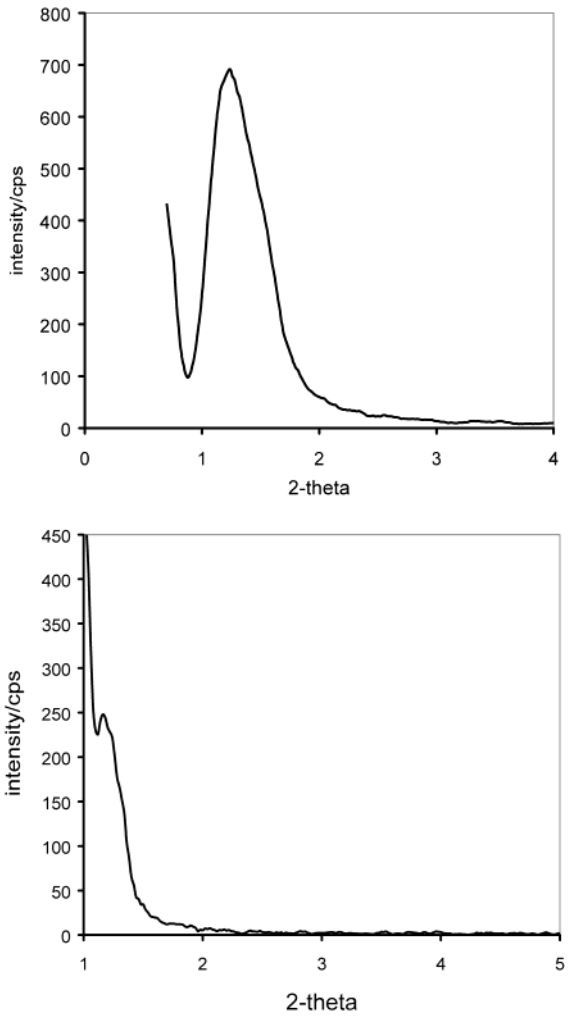

Figure 4. X-ray reflections of (a) Brij 56 and (b) Brij 78 templated nickel samples, respectively. Samples were electrodeposited at 25 °C and −900 mV vs SCE.

Electrochemical Characterization. The open circuit potential of all films was found to be approximately −0.45 V vs SCE when first transferred from the water into the KOH solution. This result is interpreted as a mixed potential due to corrosion of parts of the nickel surface, forming nickel oxide and nickel hydroxide while reducing oxygen from the solution on other regions.

(19) Bartlett, P. N.; Birkin, P. N.; Ghanem, M. A.; et al. *J. Electrochem. Soc.* **2001**, *148*, C119−C123.

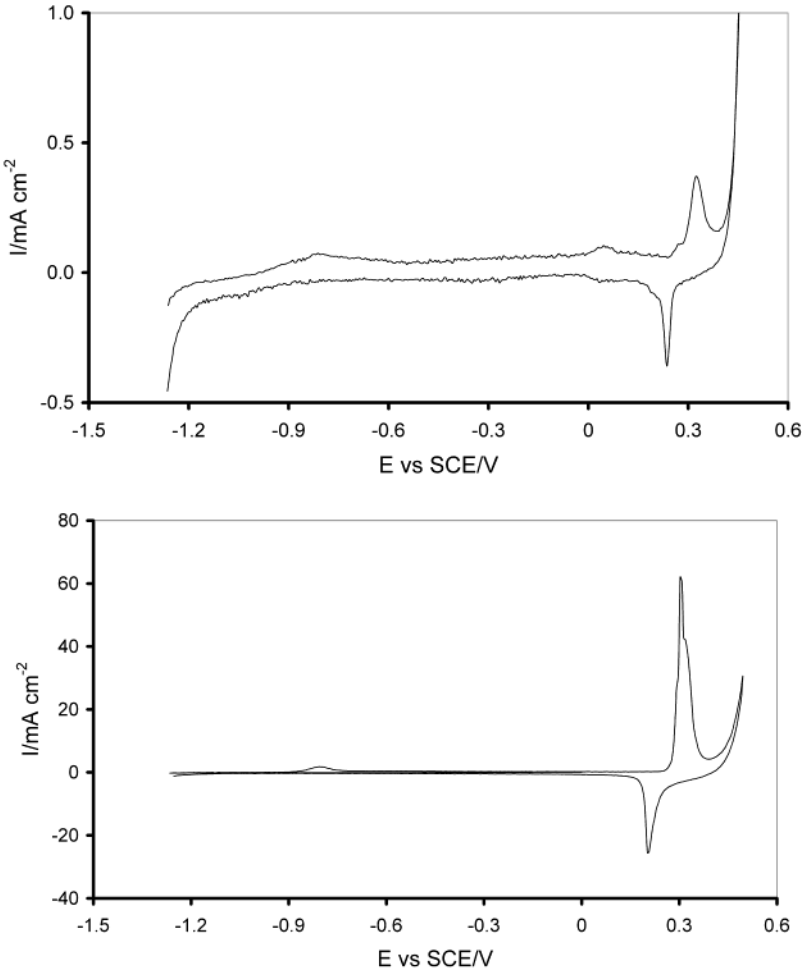

Figure 5. Cyclic voltammetry (first cycle) of (a) Ni deposited from aqueous solution and (b) Brij 56 templated mesoporous nickel in 3 M KOH (first cycle). Both samples were deposited with a charge density of 1.8 C cm^{-2} at 25 °C and −900 mV vs SCE and cycled at 20 mV s^{-1}.

The cyclic voltammogram of a film deposited from an aqueous solution containing no surfactant is shown in Figure 5a. Anodic and cathodic peaks between 0.1 and 0.4 V vs SCE with associated charges of about 1 and 0.4 mC cm^{-2}, respectively, are typical of those found in the literature and attributed to the formation and subsequent reduction of a few monolayers of Ni(OOH).[20] Previous results of nickel electrochemistry are also confirmed with a small peak at −0.8 V due to the growth of $Ni(OH)_2$ on any free nickel surface remaining after chemical oxidation,[21] followed by a shallow plateau indicating diffusion-limited growth of the same material. Previous studies have referred to thickening of the active oxide layer with surface treatments and square wave cycling or potential pulse treatment,[22,23] leading to charges of up to 30 mC cm^{-2} associated with the formation of additional NiOOH. Most authors, however, agree on a peak charge of about 0.7 to 1.0 mC cm^{-2} in this potential region during the first cycle on a smooth, clean, nickel surface.

The voltammogram of a sample grown from the Brij 56 liquid crystal template is shown in Figure 5b. The sample shows a large anodic peak at 0.26 V, with a charge of 130 mC cm^{-2}, and a cathodic peak at 0.15 V, with a charge of 50 mC cm^{-2}. The charge corresponding to the growth of $Ni(OH)_2$ by corrosion of nickel in the low potential range was very small in comparison with the peak associated with the formation of Ni(OOH) at 0.26 V. Considering that there was no surface treatment leading to oxide thickening, we can assume that the average oxide thickness was approximately the same as that for the nontemplated sample. Consequently, the increased charge is interpreted as a confirmation that the surface area available during the 20 mV s^{-1} sweep is enhanced by a factor of about 100 because of the large internal area of the pores. Unlike the case of the mesoporous platinum films reported previously,[13] where the measured charge was correlated with the adsorption of precisely one monolayer of hydrogen to obtain the surface area, the electrochemical determination of surface area in this case is complicated by the uncertainty regarding the degree of surface oxidation of nickel. Nevertheless, the observation of a large charge density confirms the expected activity due to the mesoporosity shown in the TEM.

The sharpness of the peaks in the voltammogram indicates extremely rapid charge transfer, facilitated by a highly accessible pore structure in which the diffusion of ions is rapid and unhindered. Figure 6 shows three subsequent scans at different sweep rates. The potential

(20) Amjad, M.; Pletcher, D.; Smith, C. *J. Electrochem. Soc.* **1977**, 203.
(21) Burke, L. D.; Twomey, T. A. M. *J. Electroanal. Chem.* **1984**, *162*, 101−119.
(22) Seghiouer, A.; Chevalet, J.; Barhoun, A.; Lantelme, F. *J. Electroanal. Chem.* **1998**, *442*, 113−123.
(23) Vukovic, M. *J. Appl. Electrochem.* **1994**, *24*, 878−882.

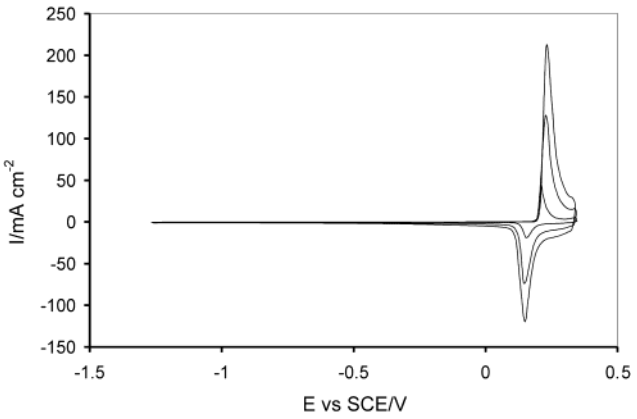

Figure 6. Cyclic voltammetry (after the first cycle) of Brij 56 templated mesoporous nickel in 6 M KOH at different scan rates: (i) 20 mV s^{-1}, (ii) 100 mV s^{-1}, and (iii) 200 mV s^{-1}.

rise to the anodic peak begins at a lower value than on the first sweep, presumably because the presence of the $Ni(OOH_x)$ structure after the first scan avoids the requirement for phase nucleation during successive scans. The linearity and scan rate independence of the leading edge of the peak suggest a resistance limitation of about 0.3 Ω cm^2 which can be attributed to the spreading resistance from the disk surface to a bulk electrolyte of conductivity 1 S cm^{-1}, that is, the rate of charging is limited only by the conductivity of the electrolyte solution. Subsequent cycles show equal anodic and cathodic charges of almost the same value as the first reduction, and the charges are also almost independent of scan rate. This confirms that the reaction rate is not hindered by diffusion in the porous network under the conditions of this experiment.

Conclusion

Thin coatings of mesoporous nickel have been electroplated from an inexpensive hexagonal phase liquid crystal template. The films contain a well-ordered pore network with spacings between 5 and 8 nm. The electrochemically accessible surface area has been estimated to be 100 times greater than samples grown without a templating electrolyte. A charge of 50 mC cm^{-2}, accessible within 1 s with an effective series resistance of less than 0.3 Ω cm^2, suggests applications in supercapacitors and pulse power devices. The high specific surface area indicates that this type of nickel coating may have a general application as a low-cost, inert, current collector for use in alkaline solution.

Acknowledgment. This work was funded by the EPSRC and the University of Southampton.

CM011021A